II International Conference on Particle-based Methods – Fundamentals and Applications
PARTICLES 2011
E. Oñate and D.R.J. Owen (Eds)

COUPLED LATTICE BOLTZMANN – DISCRETE ELEMENT METHOD FOR NUMERICAL MODELLING OF SAND PRODUCTION

ALI GHASSEMI[*] AND ALI PAK[†]

[*] Faculty of Architecture and Civil Engineering
Islamic Azad University, Qazvin Branch
Qazvin, Iran
e-mail: a_ghassemi@qiau.ac.ir, www.qiau.ac.ir

[†] Civil Engineering Department
Sharif University of Technology
Tehran, Iran
e-mail: pak@sharif.edu, www.sharif.edu

Key words: Sand Production, Lattice Boltzmann Method, Discrete Element Method.

Abstract. In this study, a coupled numerical approach based on Lattice Boltzmann Method (LBM) and Discrete Element Method (DEM) is employed for 2D simulation of fluid flow in porous media comprising of movable circular particles. The developed model is used for simulation of sand production which is one of the important problems in petroleum industry. The numerical tool has proved to have the capability of investigating the mechanisms involved in sand production problem. The results show that the rate of sand production is strongly affected by flow rate and confining pressure.

1 INTRODUCTION

A common challenge in hydrocarbon extraction from sandstone reservoirs is sand production. Production of sand particles during the oil recovery process initiates when stress changes imposed by fluid flow causes shear failure in weakly or unconsolidated rock mass near the well. It is followed by transportation of dislocated sand particles into the production well which adversely affects the well stability and disturb the pipelines and equipment. High rate of sanding may finally lead to massive sand production which blocks the well casing perforations and break the oil production. However, it has been proven that limited sand production may significantly increase the well [1].

Many researchers have attempted modelling of sand production problem through using theoretical or numerical approaches. Strong non-linear processes involved in sand production such as high changes in compressibility of rock matrix and permeability of sandstone increase the complexity of numerical simulation of this coupled hydro-mechanical phenomenon [2]. A review of modelling strategies can be found in [3].

In this paper, a newly developed numerical model has been employed to study the mechanisms influencing sand production at pore scale. Using the Discrete Element Method and the Lattice Boltzmann Method in a coupled manner, the numerical model can simulate the tortuous flow of fluid in deformable particulate media as well as capturing the destabilization

of sand arches around a perforation and the erosion process of the failed sand grains.

2 PORE SCALE MECHANICS OF SAND PRODUCTION

Sand production is resultant of a series of micro-scale processes that occurs near the casing perforations. The flow of fluid through pore spaces of rock mass imposes drag forces on the individual sand grains. The fluid properties such as viscosity and density have direct effects on the magnitude of the induced drag forces. As the hydraulic gradient of the flow is much higher near wellbore zones, the tortuous velocity of flowing fluid increases greatly, which as a result, causes higher drag forces on solid grains adjacent to the perforations. For weakly cemented sandstone, where enough cohesion resistance is not available, if the drag forces overcome the friction and interlocking between particles, sand grains may dislodge from the mass and become displaced by flowing fluid. This erosion of solid particles from porous medium makes larger canals for fluid flow and consequently increases the flux of both fluid and the produced sand particles. During the above process, sand arching may occur at the perforations near the wellbore. Forming of arches can significantly reduce the amount of produced solids. However, stability of arches is highly dependent on perforation size, particle size distribution and stress level.

Therefore, theorization of sand production problem seeks for understanding the pore scale hydro-mechanical events which dominate the behavior of the system. Despite this fact, linkages between micro-structural deformation mechanisms and observed sanding rates have not been established yet [4]. In this study, it is endeavored to investigate the role of pore scale mechanisms that are responsible for sand production.

3 COUPLED LB-DE MODEL

3.1 Background

Traditional continuum-based models such as Finite Element Method (FEM) are typically not adequate for capturing such local discontinuous behavior [3]. On the other hand, numerical models such as Discrete Element Method (DEM) in which sand grains are represented by distinct elements and their interaction can be simulated explicitly are very favorable for modeling sand production. The work of O'Connor et al. [5] is the one of the first efforts to examine the ability of DEM to model the mechanics of sand production. Dorfmann et al. [6] utilized a DEM model to simulate the sand production and arching effects around a cavity. In their study, capillary forces between adjacent grains were included in the DEM model to compare the effect of pressure gradient and capillary forces on the formation of stable arch configuration around a cavity. Jensen et al. [7] modeled sand production using the coupling of two dimensional DEM and finite element implementation of the two-dimensional continuity equation for Darcy flow. Their simulation shows that as the strength of the cohesive bonds decreases, the number of particles breaking free from the matrix increases.

To represent fluid–solid interaction at the local scale, it is more delicate to simulate the fluid flow in the pore space at a resolution finer than that of pores and grains [8]. Among a number of microscpic numerical methods in the context of computational fluid dynamics, Lattice Boltzmann Method (LBM) has proven to be a versatile method for simulation of fluid flow in systems with complex solid boundary conditions such as porous media. The particle-

like nature of LBM permits a transparent handling of irregular flow paths through particulate media using elementary mechanical events such as mirror and bounce-back reflections without comprising great computational costs. Coupled LB-DE model was first introduced by Cook [9]. In the coupling scheme, the velocity of the fluid adjacent to solid surfaces is set to velocity of solid to retain the no-slip boundary condition. The two-dimensional LB-DE model has been validated through a number of benchmark problems including Coutte flow, particle sedimentation and drafting-kissing-tumbling phenomenon [9, 10]. Recently, the coupled LB-DE model was applied for modeling simplified forms of some engineering issues such as sand boiling in granular soils [11], vacuum dredging [12] and sand production [4].

3.2 Theoretical aspects of coupled LB-DE model

Discrete Element Method

Discrete element method (DEM has become a powerful numerical tool for analyzing particulate media since it was first introduced by Cundall & Strack [13]. The discrete element method conceives granular materials as an assemblage of distinct rigid particles. Solid rigid particles can interact among each other or with solid boundaries when overlap of boundaries occurs between particle/particle or particle/wall. By using the contact-force displacement law, the forces at contacts are related to the magnitude of the overlaps. The displacement and velocity of each individual solid particle are calculated from the summation of all forces acting on the particle using Newton's second law of motion. This calculation cycle is performed in each time step during the analysis.

The force-displacement law establishes a relationship between the contact force and the magnitude of particle overlap by the following equations:

$$\Delta F_n = K_n \Delta_n \quad ; \quad \Delta F_t = K_t \Delta_t \tag{1}$$

where ΔF , K , and Δ are incremental force, stiffness, and magnitude of particle overlap, respectively. The subscripts n and t represent normal and tangential directions with respect to the plane of particle overlap. Then, contact forces between each two contacting particles are updated:

$$F_n^{t+\Delta t} = F_n^t + \Delta F_n \quad , \quad F_t^{,t+\Delta t} = F_t^t + \Delta F_t \tag{2}$$

The tangential contact forces are usually governed by some frictional relationships. The Coulomb criterion was adopted in this study. Accordingly, the commencement of slippage occurs where the tangential contact force exceeds the following criterion:

$$F_{c,j}^{\ t,\max} = \mu_s F_{c,j}^{\ n} + c \tag{3}$$

where μ_S is the sliding friction coefficient between two contacting solid particles and $F_{c,j}^{\ n}$ and $F_{c,j}^{\ t}$ are the normal and tangential contact forces on particle j.

Newton's second law of motion describes the relationship between the acting forces and the movement of particles. The 2D form of this law which has been applied in the developed DEM code for current study is given by:

$$m_j \ddot{x}_{ij} = \sum F_{ij} \tag{4}$$

$$I_j \ddot{\theta}_j = \sum M_j \tag{5}$$

where $\ddot{x}_{i,j}$ and $\ddot{\theta}_j$ are linear and angular accelerations of particle j at direction i and m_j and I_j are the mass and moment of inertia of discrete particle j, respectively.

A few models have been proposed for incorporating the rolling resistance in DEM, which can be classified into two categories: angular-velocity-dependent and -independent, as have been discussed by Zhu & Yu [14]. Herein, the angular-velocity independent model was chosen because it is simpler and more effective.

Based on the modified algorithm, Equation (5) can be rewritten as follows:

$$I_j \ddot{\theta}_j = \Sigma \left[(F^t_{c,j} \times R_j) - \mu_r R_j \left| F^n_{c,j} \right| \lambda + M_{nc,j} \right] \quad , \quad \lambda = sign\,(F^t_{c,j}) \tag{6}$$

where R_j is the radius of particle j, μ_r is the rolling fiction coefficient and $M_{nc,j}$ is the part of moment on particle j which is induced by non-contact forces. μ_r is a dimensionless parameter which is dominated by roundness of contacting particles.

Lattice Boltzmann Method

Unlike the traditional CFD methods that directly solve the Navier-Stokes equations, LBM actually simulates macroscopic flows by means of a particulate approach. LBM was applied to porous flow soon after its emergence in 1989 [15]. Later studies confirmed the reliability of LBM in modeling flow through porous media (e.g. Pan et al. [16] and Ghassemi & Pak [17]).

In LBM, the spatial space is discretized in a way that it is consistent with the kinetic equation. In this method, space is divided into regular lattices with the same spacing h in both x- and y-directions and at each lattice site a particle distribution function $f_m(x,t)$ is defined which is equal to the expected number of identical fluid particles at that site x in the direction of m. During each discrete time step of the simulation (Δt_{LB}), fluid particles move to the nearest lattice site along their direction of motion with different velocities of $\vec{e}_m$, where they "collide" with other bundles of fluid particles that arrive at the same site. The outcome of the collision is determined by solving the Boltzmann equation for the new particle distribution function at that site and the particle distribution function is updated. The magnitude of speed in different directions which is called lattice speed is defined as $C = h / \Delta t_{LB}$.

Propagation and collision of fluid particles in LBM can be mathematically summarized by the below two-step scheme, respectively:

$$f_m(x + \vec{e}_m \Delta t, t + \Delta t) = f_m(x,t) \tag{7}$$

$$f_m^{updated}(x,t) = \Omega_m(f(x,t)) \tag{8}$$

The collision rule Ω should be chosen to leave the sum of the $f_m(x,t)$ unchanged (no fluid particles are lost.) The rule is also selected to conserve the total momentum at each lattice site.

The single relaxation time BGK (after Bhatnagar, Gross, and Krook [18]) operator approach is an uncomplicated approach which simply approximates the collision by assuming that the momenta of the interacting fluid particles will be redistributed at some constant rate toward an equilibrium distribution f_m^{eq} . BGK allows one to solve the equilibrium distribution such that the microscopic equations are satisfied and the Navier-Stokes equations are recovered. In BGK lattice Boltzmann method, collision rule is given by:

$$\Omega_m(x,t) = f_m(x,t) - \frac{\Delta t_{LB}}{\lambda}(f_m(x,t) - f_m^{eq}(x,t)) \tag{9}$$

where f_m^{eq} is the local equilibrium density distribution for the fluid and λ is relaxation parameter. The two-dimensional model implemented in this study uses a square, nine-velocity lattice typically referred to as D2Q9 model. For this model, f_m^{eq} is given by [19]:

$$f_0^{eq} = w_0 \rho (1 - \frac{3}{2C^2} \vec{V}.\vec{V}) \tag{10}$$

$$f_m^{eq} = w_m \rho \left[1 + \frac{3}{C^2}(\vec{e}_m.\vec{V}) + \frac{9}{2C^2}(\vec{e}_m.\vec{V})^2 - \frac{3}{2C^2}(\vec{V}.\vec{V}) \right], \quad m = 1,2,...,8 \tag{11}$$

in which ρ and V are macroscopic fluid density and velocity and w_m are the fixed weighting values: $w_0 = \frac{4}{9}; \quad w_{1,2,3,4} = \frac{1}{9}, \quad w_{5,6,7,8} = \frac{1}{36}$

The macroscopic parameters are regained by:

$$\rho = \sum_{m=0}^{8} f_m \quad , \quad \rho \vec{V} = \sum_{m=1}^{8} f_m \vec{e}_m \tag{12}$$

The dimensionless relaxation parameter $\tau = \lambda / \Delta t_{LB}$ is related to the fluid viscosity by:

$$\nu = \frac{1}{3}(\tau - \frac{1}{2}) \frac{h^2}{\Delta t_{LB}} \tag{13}$$

Coupling approach

In this study, a weakly coupling scheme similar to what has been used by Cook [9] is employed. During each time step, the LB code is called to simulate the fluid flow and the hydrodynamic forces and moments on individual particles are calculated and then exported to DEM as input data. In DEM, the fluid-induced forces are combined with other existing forces acting on particles to determine the new position of particles. Since the time step for LB in our simulations is always greater than the time step for DE, each LB calculation cycle is accompanied with a number of DEM calculation cycles during which the hydrodynamic forces are unchanged.

Different methods are available in LB literature for obtaining hydrodynamic forces acting on the particles moving on the LB lattice [20, 21 and 22]. Herein, the immersed moving boundary method [21] was employed since it has been successfully applied and verified by majority of previous researches on DE-LB simulations [9, 10, 23]. In this method, the collision rule (Equation (9)) is modified to incorporate the influence of the solid particles:

$$f_i(x + e_i\Delta t, t + \Delta t) = f_i(x,t) - \frac{1}{\tau}(1 - B)[f_i(x,t) - f_i^{eq}] + Bf_i^m \tag{14}$$

For each lattice node, weighting parameter B is defined as a function of solid ratio which is the ratio of area occupied by solid to the total area of the $h \times h$ computational cell around the lattice node [23]. f_i^m is an additional collision term that bounces back the non-equilibrium part of the distribution which is given by Cook [9] as:

$$f_i^m = f_i^{eq}(\rho, v_b) - f_{-i}^{eq}(\rho, v_b) + f_{-i}(x,t) - f_i(x,t) \tag{15}$$

where v_b is the velocity of the solid and the subscript $-i$ indicates the direction opposite to i. According to this approach, the fluid induced hydrodynamic force and torque on a solid particle mapped on n lattice nodes is calculated by the following equations, respectively:

$$F = Ch\left[\sum_n (B_k \sum_i f_i^m e_i)\right] \tag{16}$$

$$T = Ch\left[\sum_n (x_k - x_c) \times (B_n \sum_i f_i^m e_i)\right] \tag{17}$$

where x_k and x_c are the coordination of node k and center of particle, respectively.

2D LB modeling of fluid flow through compacted particulate samples in which solid particles are in physical contact with neighboring particles may not be efficient because there may be inadequate interconnected pores to allow the fluid particles to flow through the 2D system. This problem can be solved numerically by using hydraulic radius multiplier technique. In this approach, the mechanical radius of particles is reduced in LB simulations to resolve the flow of the fluid through the sample [4]. The hydraulic radius is only considered for LB code and the real (mechanical) radius is still used in DE calculations.

Verification of the developed coupled LB-DE code has been discussed elsewhere [24]

4 NUMERICAL MODELING OF SAND PACK EXPERIMENT

4.1 Sand pack experiment

In the present study, a series of sand pack experiments conducted by Al-Awad et al. [25] was considered for numerical simulation by the developed model. In sand pack tests, a viscous fluid permeates through a confined cylindrical sand sample at one end, thereby inducing sand production at the other end through a small orifice. In their work, sand packs were constructed analogous to samples obtained from certain reservoir and they studied the amount of sand production under different conditions of flow rate and confining pressure. The sand packs had an inside diameter of 3.81 cm and 8 cm length and the diameter of the orifice is 4 mm. The porosity of all constructed samples was about 0.45.

4.2 Numerical simulation

Numerical modeling of the whole sand pack is not currently possible because of high

computational costs. Therefore, only part of sample near the outlet of sand box was considered for numerical simulation as depicted on Figure 1. Thus, the model may not be able to simulate the complete sand production cycle in which production of sand stops after development of a stable cavity especially for higher flow rates. Despite this shortcoming, the numerical model is capable of predicting the onset of sanding and rate of sand production at early time of production.

The sand sample for numerical simulations was created by particle packing technique using DEM [17]. The porosity of the created sample was about 0.16 and the grain size distribution of the sample is shown in Table 1. Because of 2D nature of the model, this porosity cannot directly be compared with that of the real sample. In turn, porosity of the model can be adjusted by changing the hydraulic radius multiplier (sec. 3-2) in a manner that the intrinsic permeability of the sample is equivalent to that of real porous medium.

For coupled analyses, a difference in fluid pressure was applied at two opposite sides of the soil sample in order to induce the flow towards the outlet, and the other two sides are treated as no-slip boundaries. Discretization of the domain needs to be fine enough in order to adequately resolve the fluid flow in the numerous small pores created by the finest solid particles, and also to provide adequate resolution for smooth variations of hydrodynamic forces when solid particles are moving on the fluid lattice. In this work, lattice spacing varied between 0.012 to 0.018 mm in different analyses. The values of other LB parameters used in this study are listed in Table 2.

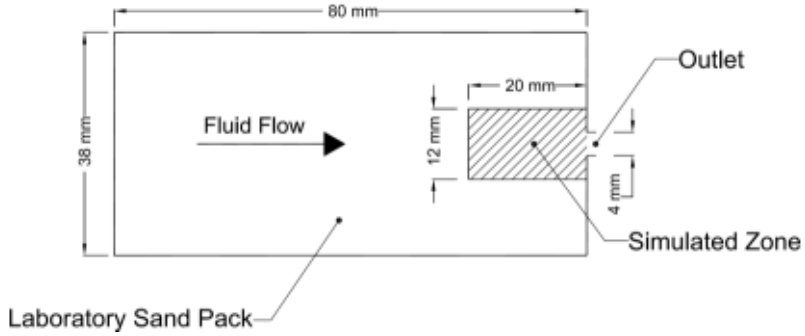

Figure 1: Dimensions of laboratory sand pack and simulation domain

Table 1: DEM parameters

Prameter	Value
No. of particles	7500
D (mm) [weigth percentage %]	0.6 [2], 0.3 [43], 0.25 [20], 0.125 [35]
ρ_s (kg/m^3)	2600
Kn , Ks (N/m)	10^7
μs , μr	1.0, 0.2

Table 2: LBM parameters

Prameter	Value
h (mm)	0.018,0.014,0.012
τ	0.52
ν (m^2/s)	1.05×10^{-5}

The main DEM parameters used for simulation of sand erosion is gathered in Table 1. High values of friction coefficients were chosen to compensate for the low shear strength of the assembly of circular disks comparing to the real sand pack which contains grains with irregular shapes. However, early numerical results showed that a small value for interparticle cohesion is also required to artificially simulate the absence of interlocking resistance between circular particles in the numerical model. Constant stress boundary condition was applied for the top, bottom, and left walls using a servo-control approach in which the walls are allowed to displace in order to retain the required constant stress level on the walls.

5 RESULTS AND DISCUSSIONS

Prevailing failure mechanism for sand production depends on the values of in situ effective stresses and flow rate in relation to rock strength [26]. For weak sandstone, sand is produced when drag forces caused by flowing fluid exceed the formation strength which is mainly supplied by true cohesion of natural cementing materials, resistance developed by inter-particle friction controlled by normal contact forces, and the apparent cohesion induced by interlocking between sand grains. For unconsolidated rock mass, the true cohesion is not available and rock resistance against erosion of sand grains by fluid induced forces (tensile failure) can only be attributed to inter-particle forces and interlocking between sand grains.

From the above discussion, for condition of the sand pack experiment considered for numerical simulation in this study (where no cementing material exist in the sample), the level of drag forces induced by fluid flow as well as inter-particle forces governed by applied confining pressure around the sample are the most important factors influencing the sanding initiation through the small perforation. In the following sections, the results of numerical analyses for different conditions of flow rates and confining pressures are discussed.

5.1 Effect of flow rate

The results of some of the analyses in terms of cumulative weight of the produced sand versus time for two different applied pressure gradients are shown in Figure 2. The quantity of the produced sand has been calculated from the number of solid grains passing the orifice. Initial high rate of sand production at the early times of simulation (before 0.05 s) for both cases is due to the exit of sand particles in the vicinity of the orifice immediate after removing the wall. However, for lower pressure gradient ($\nabla p = 0.10\ MPa/m$), formation of stable cavity around the perforation caused stopping the sand production, for higher pressure gradient ($\nabla p = 0.44\ MPa/m$) sand production continues up to end of the simulations. The variation of flow rate with time was also plotted on the figures. For lower pressure gradient (Figure 2a), the flow rate is almost unchanged after formation of stable cavity. However, for higher pressure gradient (Figure 2b), sand production continues with a decreasing rate implying that the cavity is propelled gradually towards steady conditions; simultaneously, the flow rate is gradually increased to about 1.5 times the initial flow rate. Therefore, it may be concluded that high flow rate with limited sand production can be obtained by applying appropriate pressure gradient. Extension of this deduction to production in oil reservoirs leads to suggestion of allowing limited amount of sand production for increasing the oil productivity which has been recently considered by petroleum industry [27].

Figure 3a and b show the variation of cumulative weight of produced sand with time for

different values of flow rates while confining pressure was kept constant at 0.4 and 2.5 MPa, respectively. As can be seen, the numerical model predicts the increase of sand production where higher rates of fluid flow occur.

The normal production status in oil reservoirs is that, a well may produce a uniform amount of sand independent of production rate until some critical production rate is exceeded. Determination of critical flow rate is very important, because increasing the production rate above the critical rate results in strong increase of sand production rate. Critical flow can be determined from the results of numerical simulations by perusing the variation of the produced sand versus flow rate at different simulation times as depicted in Figure 4. From this figure, for flow rates higher than about 100 mm3/s, the rapid increase in weight of the produced sand with time indicates that the flow rate exceeds the critical flow rate while confining pressure is equal to 0.4 MPa.

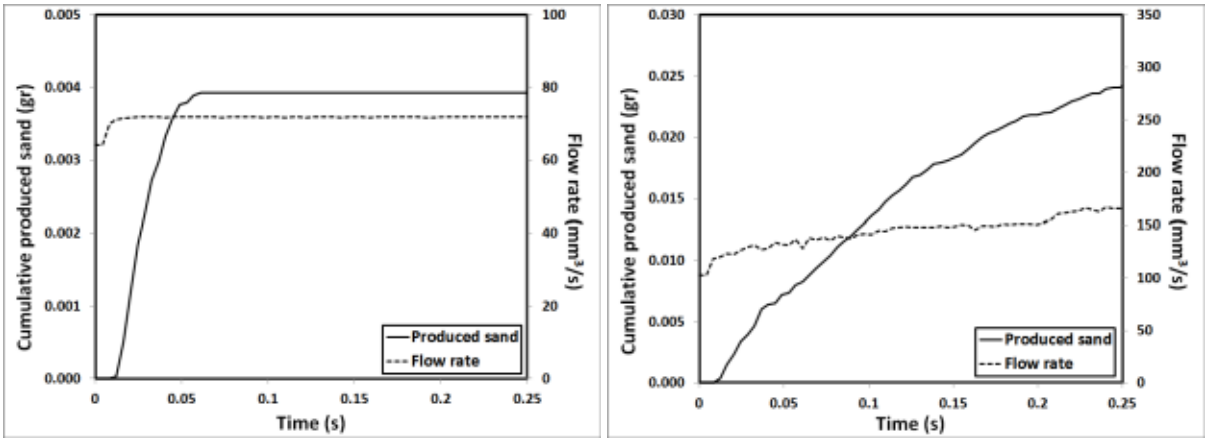

(a) $\nabla p = 0.10\ \ MPa\ /m$ (b) $\nabla p = 0.44\ \ MPa\ /m$

Figure 2: Comulative weight of produced sand versus time for two different applied pressure gradient

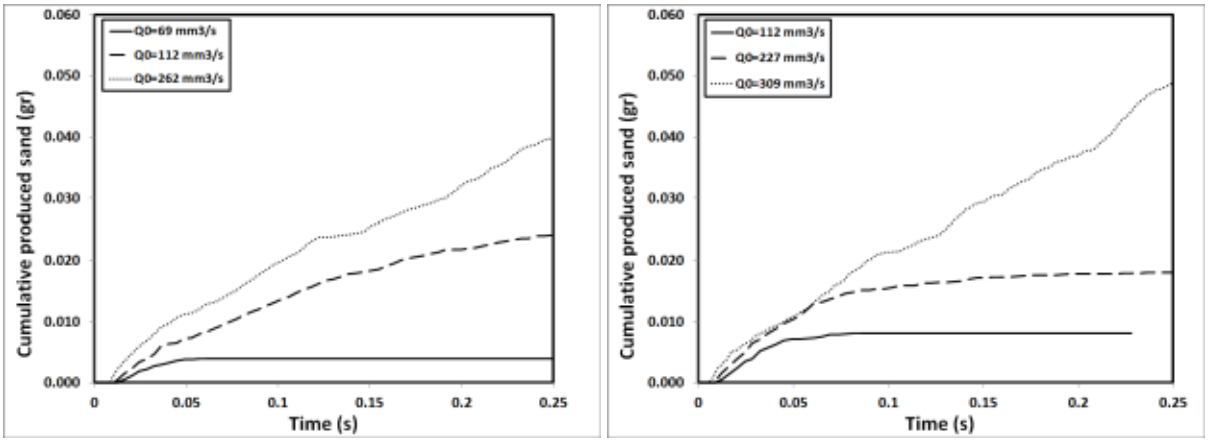

(a) 0.4 MPa (b) 2.5 MPa

Figure 3: Comulative weight of produced sand versus time for two different applied confining pressure

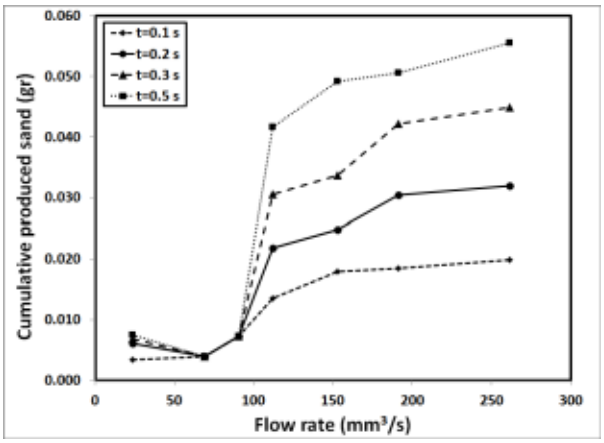

Figure 4: Variation of the weight of produced sand with flow rate at different simulaion times

5.2 Effect of confining pressure

Previous studies show that the effect of confining pressure on arching behavior is a function of grain size distribution, particles size and dimension of the outlet opening [28, 29]. Generally speaking higher confining stresses causes increased shear strength which results in higher frictional resistance between sand particles and improving the arch stability.

The effect of confining pressure on the value of critical flow rate was studied by further analyses for two other confining stresses (2.5 and 4.4 MPa). Comparison between the results for different confining stresses (Figure 4, 5a and 5b) implies that for higher confining stresses, the rate of sand flow has been reduced. Also, the results obtained by numerical model confirm increasing the critical flow rate when higher confining pressures are applied. In Figure 6, the results of numerical simulations were compared with Al-Awad et al.'s experimental observations. Both of the curves show that increasing the confining pressure results in increasing in the critical flow rate. The higher slope of numerical curve in this figure implies that the numerical model slightly overestimates the effect of confining pressure. The reason for this different may be the 2D nature of the numerical modeling which confines the sand particles more than what occurs in the physical experiments.

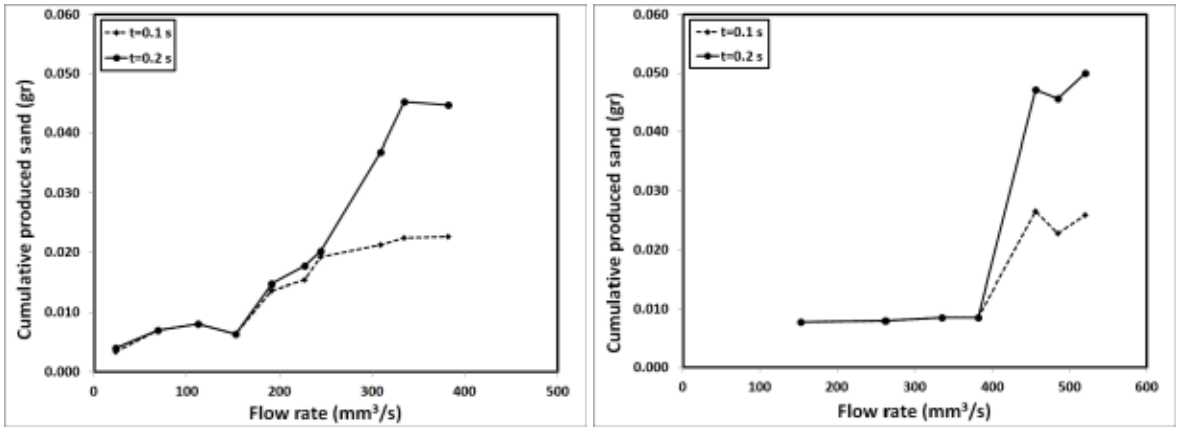

(a) 0.4 MPa (b) 2.5 MPa

Figure 5: variation of the weight of produced sand with flow rate at different simulaion times

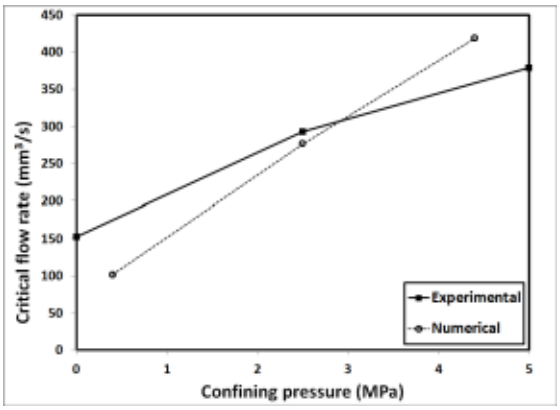

Figure 6: Critical flow rate for different confining pressures

6 CONCLUSIONS

A coupled LB-DE model has been developed which is capable of capturing the fundamental mechanisms involved in sand production phenomenon. By using the developed code, it becomes possible to evaluate the effects of different parameters on the sand production rate/volume such as flow rate and confining stresses. Based on the conducted numerical simulations explained above, the following conclusions can be drawn:

1) The numerical model predicts the increase of sand production where higher rates of fluid flow occur.

2) The obtained results show that increasing the confining pressure results in increasing the critical flow rate which confirms the experimental observations.

REFERENCES

[1] Wang J., Walters D., Settari A. and R.G. Wan. An integrated modular approach to modeling sand production and cavity growth with emphasis on the multiphase flow and 3D effects. *41st U.S. Symposium on Rock Mechanics*, Golden, Colorado, (2006).

[2] Dusseault M. Coupled processes and petroleum geomechanics, *Coupled Thermo-Hydro-Mechanical-chemical processes in geo-systems*, Elsevier geo-eng. book series (2004).

[3] Wang J. and D.D. Joseph Lift forces on a cylindrical particle in plane Poiseuille flow of shear thinning fluids. *Phys. Fluids*. (2003)18(8), 2267-2278.

[4] Boutt, D.F., Cook, B.K., and J.R. Williams A coupled fluid-solid model for problems in geomechanics: application to sand production. *Int. J. Anal. Numer. Meth. Geomech.* (2010).

[5] O'Connor, R., Torczynski, J. R., Preece, D. S., Klosek, J. T. and J.R. Williams Discrete Element Modeling of Sand production. *Int. J. Rock Mech. & Min. Sci.* (1997) pp. 34-44.

[6] Dorfmann A.; Rothenburg L. and M.S. Bruno Micromechanical modeling of sand production and arching effects around a cavity. *Int. J. Rock Mech. & Min. Sci.* (1997) Vol. 34, No. 3-4.

[7] Jensen, R., D. Preece, B. Cook, E. Perkins and J. Williams Coupled Fluid-flow/particle-motion Computer Modeling of Sand Production in Oil Wells. SPE No 56630 (1999).

[8] Han Y. and Cundall P.A. Lattice Boltzmann modeling of pore-scale fluid flow through idealized porous media. *Int. J. Anal. Numer. Meth. Fluids*. (2010) DOI: 10.1002/fld.2443.

[9] Cook, B.A. Numerical framework for the direct simulation of solid-fluid systems. *PhD thesis* (2001), MIT.

[10] Cook B, Noble D and J. Williams A direct simulation method for particle-fluid systems. *Engineering Computations* (2004) 21, 151–168.
[11] Mansouri M., Delenne J.-Y., El Youssoufi M.S. and A. Seridi A 3D DEM-LBM approach for the assessment of the quick condition for sands, *C. R. Mecanique* (2009) 337, 675–681.
[12] Feng Y.T., Han K. and D.R.J. Owen Combined three-dimensional lattice Boltzmann method and discrete element method for modelling fluid–particle interactions with experimental assessment. *Int. J. Numer. Meth. Engn* (2010), 81:229–245.
[13] Cundall P. and O.D.L. Strack A discrete numerical model for granular assemblies. *Geotechnique* (1979) 29(1), pp. 47–65.
[14] Zhu, H.P., Yu A.B. A theoretical analysis of the force models in discrete element method. *Powder Technology* (2006) 161, pp. 122–129.
[15] Succi S., Foti E., and F. Higuera Europhys. Lett. (1989) 10, 433.
[16] Pan, C., Luo L. and C. Miller An evaluation of lattice Boltzmann schemes for porous medium flow simulation. *Computers & Fluids* (2006) 35, 898–909.
[17] Ghassemi A., Pak A. Pore scale study of permeability and tortuosity for flow through particulate media using Lattice Boltzmann method, *Int. J. Anal. Numer. Meth. Geomech.*, (2011) 35(8), 886–901.
[18] Bhatnagar, P. L., Gross, E. P. and Krook, M. A model for collisional processes in gases I: small amplitude processes in charged and neutral one-component system. *Phys. Rev.* (1954), 94, 511.
[19] Qian Y., d'Humieres D. and P. Lallemand Lattice BGK models for Navier–Stokes equation. *Europhysics Letters* (1992) 17:479–484.
[20] Ladd A. Numerical simulations of fluid particulate suspensions via a discretized Boltzmann equation (Parts I & II). *Journal of Fluid Mechanics* (1994) 271:285–339.
[21] Noble D. and Torczynski J. A lattice Boltzmann method for partially saturated cells. *International Journal of Modern Physics C* (1998) 9:1189–1201.
[22] Inamuro T., Maeba K. and F. Ogin Flow between parallel walls containing the lines of neutrally buoyant circular cylinders. *Int. J. of Multiphase Flow* (2000) 26, 1981-2004.
[23] Feng Y.T., Han K. and D.R.J. Owen Coupled lattice Boltzmann method and discrete element modeling of particle transport in turbulent fluid flows: Computational issues. *Int. J. Numer. Meth. Engng* (2007) 72:1111–1134.
[24] Ghassemi A. *PhD thesis* (2011) Sharif Universityy of Technology, Tehran, Iran.
[25] Al-Awad M.N.J., El-Sayed H. and Desouky S.E.M. Factors affecting sand production from unconsolidated sandstone Saudi oil and gas reservoir. J. King Saud Univ. (1999) vol.11, Eng. Sci. (1), pp.151-174.
[26] Nouri A. A comprehensive approach to modeling and eliminating sanding problems during oil production. *PhD thesis*, Dalhouse University, (2004).
[27] Vaziri H. H., Lemoine E., Palmer I.D. and R. Islam How Can Sand Production Yield a Several-Fold Increase in Productivity: Experimental and Field Data. SPE63235 (2000).
[28] Hall C.D., hariisberger W.H. Stability of sand arches: a key to sand control. *Journal of Petroleum Technology* (1970) pp.821-829.
[29] Miller W.G. Sand flow mechanisms at well casing perforations. *Ms.c. Thesis* (1994), University of Alberta.